Modeling Arthropod Filiform Hair Motion using the Penalty Immersed Boundary Method

J. J. Heys[1] T. Gedeon[2] B.C. Knott[1] Y. Kim[3]

[1] Chemical Engineering Department, Arizona State University, Tempe, AZ

[2] Department of Mathematical Sciences and Center for Computational Biology, Montana State University, Bozeman, MT

[3] Courant Institute, New York University, NY

February 15, 2007

Abstract

Crickets are able to sense their surrounding environment through about 2000 filiform hairs located on a pair of abdominal cerci. The mechanism by which the cricket is able to sense a wide range of input signals using these filiform hairs of different length and orientation is of great interest. Most of the previous filiform hair models have focused on a single, rigid hair in an idealized air field. Here we present a model of the cercus and filiform hairs that are mechanically coupled to the surrounding air, and the model equations are based on the penalty immersed boundary method. The key difference between the penalty immersed boundary method and the traditional immersed boundary method is the addition of forces to account for density differences between the immersed solid (the filiform hairs) and the surrounding fluid (air). The model is validated by comparing the model predictions to experimental results, and then the model is used to examine the interactions between multiple hairs. With multiple hairs, there is little interaction when the hairs are separated by more than 1 mm, and, as they move closer, they interact through viscous coupling, which reduces the deflection of the hairs due to the air movement. We also examine the computational scalability of the algorithm and show that the computational costs grow linearly with the number of hairs being modeled.

Keywords: immersed boundary, fluid-structure interaction, arthropod filiform hairs, penalty method, crickets

1 Introduction

Crickets share many of the same sensory requirements of other living organisms. They must be able to sense the surrounding environment with a sufficient fidelity that they can detect the presence and location of predators and find a mate. To achieve these requirements, crickets and many other arthropods have thread-like hairs called filiform hairs (see figure 1) that move in response to

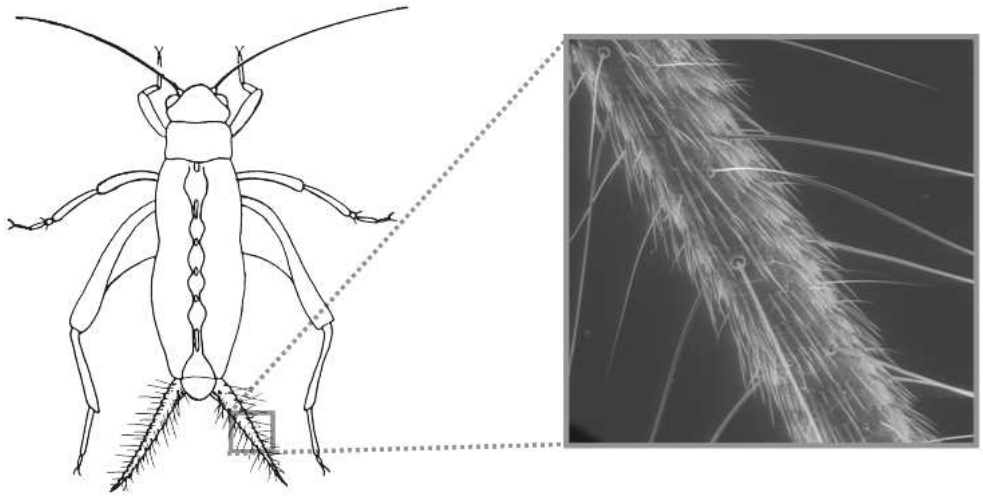

Figure 1: **Filiform Hairs on the Cricket Cercus**. The cricket has a pair of abdominal cerci that contain 1000-2000 filiform hairs each.

viscous forces from the surrounding air. For adult crickets, these wind-receptor hairs are located on a pair of abdominal cerci, which contain 1000 - 2000 filiform hairs each [15]. The length of the wind-receptor hairs vary between 30 and 1500μm [13], and the hair density is higher near than abdomen relative to the posterior end of the cercus. The hair diameter varies not only between different hairs (from 1 to 9μm), but also from the tip to the base (with the square root of distance from the tip, [13]). Even though the size and shape of the filiform hairs is highly variable, the inter-animal variability is apparently extremely low. Among adult crickets, the number of filiform hairs is nearly identical, and each hair's length, position, and directional movement plane vary at most by 5% across different individuals [12, 25, 24]. At the base of each filiform hair is a single mechanoreceptor neuron that senses the deflection of the hair. Since the motion of each filiform hair is restricted to a single plane, the cricket receives information about the velocity, frequency, and direction of air movement through the filiform hairs.

Crickets utilize this wind-sensitive system for a number of different purposes. They posses a well-known ability to communicate acoustically through chirp activities. Non-acoustic communication is used by male crickets that generate traveling vortex rings using a wing flick during aggressive encounters and courtship [9]. The system is also of critical importance for predator avoidance and oriented escape running [6, 8, 7, 18]. It is ultimately the differences in both the filiform hair structure and cerci structure that enable this wide range stimuli to be perceived.

A number of mathematical models have been developed to help describe the relationship between

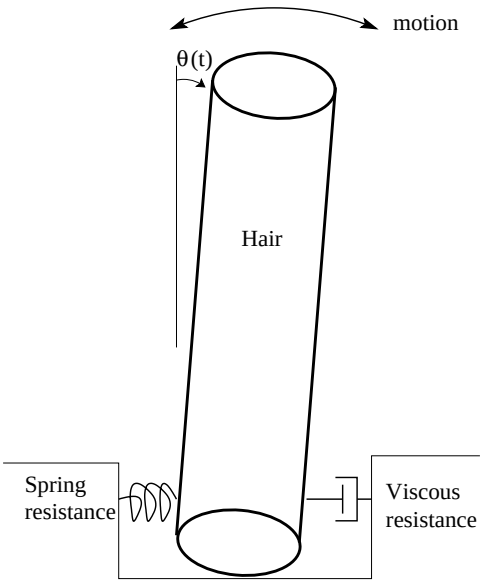

Figure 2: **Inverted Pendulum Model**. An early model of filiform hair motion utilized an inverted pendulum with spring- and viscous-resistance elements.

filiform hair structure and its response to various stimuli. One of the earliest models was proposed in a series of papers by Shimozawa and Kanou [24, 23]. The model was developed by assuming that the filiform could be approximated as an inverted, rigid pendulum with both a viscous- and a spring-type elements to resist angular displacement as shown in figure 2. The equation of motion describing the motion of the filiform hair under this assumption is

$$I \cdot \frac{d^2\theta}{dt^2} + R \cdot \frac{d\theta}{dt} + S \cdot \theta = N, \tag{1}$$

where I is the moment of inertia of the hair, R is the viscous resistance within the hair base, S is the spring stiffness, and N is the torque applied by the moving air. The R and S parameters where determined through experiments on filiform hairs, and N was approximated using Stokes's solution to flow above a large oscillating plate. In other words, the cercus was approximated as a large plane without any obstructions (e.g., hairs).

The model of Shimozawa and Kanou was modified by Humphrey *et al.* in a later series of papers [10, 1, 4]. The main differences between the models are the addition of a 'virtual mass' term that captures the effects of fluid inertia and the use of an alternative theory (also by Stokes) for estimating the drag force on the pendulum. The virtual mass term is only significant when the surrounding fluid is a liquid because gaseous surrounding fluids have a Reynolds number less than

1 so fluid inertia is likely to be negligible. The new drag force estimate was a significant change to the model because, for example, it modeled the cercus as a cylinder. However, the cercus in the Humphrey model is still smooth and there are no interactions between the hairs.

Improvements to the Humphrey model have been proposed. Shimozawa et al.[12, 25] examined the effects of varying the filiform hair shape, and, recently, Bathellier et al. [2] developed methods for modifying the idealized flow field around a hair to approximate the viscous dampening of the hair on the fluid in order to approximate hair-to-hair coupling. Most recently, Cummins et. al. [3] developed the first comprehensive model for the study of fluid mediated viscous interaction between an arbitrary number of hairs. Their model builds on Humphrey model in treating the cercus as an infinite cylinder and allowing only periodic fluid motion in the axial direction. The fluid velocity is then the sum of the explicit solution for oscillating flow over an infinite cylinder (without hairs) and a perturbation velocity due to the presence of hairs. The perturbation velocity is computed using the Stokes flow approximation to Navier-Stokes equations. Because of this approximation the model is accurate only for low and moderate frequencies of the driving fluid and for relatively short distances between the hairs.

In summary, the following assumptions are generally used in deriving models of filiform hair motion:

1. the hairs are rigid, linear oscillators,
2. angular motion of the hair is restricted by a viscous- and spring-type resistance elements at the base,
3. the cercus is a smooth cylinder or infinite plane,
4. often, there is no hair-to-hair interaction, and
5. the bulk flow is oscillatory.

The model of the cercus and filiform hairs presented in the next section was developed to avoid making some of the assumptions in the Humphrey and Cummins models. Specifically, arbitrary driving flow from any direction is allowed, the hairs do not have to be completely rigid, and the bulk flow is determined by solving the Navier-Stokes equations using a second-order accurate method. The hair-to-hair viscous coupling is also captured. These advantages are bringing us closer to the long-term goal of improving our understanding the environmental and functional constraints under

which the cercus system operates. In the short term we can study the important question of fluid-mediated interaction between the hairs. On what spatial scale is this interaction non-negligible? How does it depend on the relative lengths, positions and other characteristics of interacting hairs? Bathelier et. al. [2] and Cummins et. al. [3] both studied these questions using their respective approximations and we address this question in section 3.2. While bulk oscillatory flow is an important problem, there are examples of small scale flow structures, such as microturbulence, being used for communication. Eventually, a model that can capture these structures in the fluid may improve our understanding of cricket-to-cricket communication. Our model is a step in this direction.

2 Penalty Immersed Boundary Method

The equations of motion for a three-dimensional viscous incompressible fluid are [20]

$$\rho\left(\frac{\partial \mathbf{u}}{\partial t} + \mathbf{u}\cdot\nabla\mathbf{u}\right) = -\nabla p + \mu\Delta\mathbf{u} + \mathbf{f}, \tag{2}$$

$$\nabla\cdot u = 0, \tag{3}$$

where $\mathbf{u}$ and p are the velocity and pressure of the fluid. At 20^oC the viscosity (μ) and density (ρ) of air are $1.8\times10^{-5}\ kg/(m\,s)$ and $1.2\ kg/m^3$ respectively. Selecting a characteristic velocity, V_0, of $0.01\ m/s$ and a characteristic length scale, L, of $1\times10^{-3}\ m$ gives a Reynolds number of

$$Re = \frac{L\,V_0\,\rho}{\mu} = 0.67. \tag{4}$$

A more appropriate characteristic length scale may be the diameter of the hair ($L = 5\times10^{-6}\ m$), which gives $Re = 3.3\times10^{-3}$. In either case, the $\mathbf{u}\cdot\nabla\mathbf{u}$ term on the right side of equation 2 is likely to be small, but it will be retained because it does not contribute significantly to the computational costs of the algorithm employed here. The body force term, $\mathbf{f}$, on the left side is going to be significant in what follows because this term will capture the effects of the immersed, elastic boundary with mass.

The immersed boundary method [19, 21, 14, 20] treats the entire domain as a fluid. One- and two-dimensional boundaries without any volume are then 'immersed' in that fluid and coupled to the fluid through a force balance and a velocity matching condition. Originally, the immersed

boundary method was developed to model the interaction between a tissue and a biological fluid. Because tissues typically have a density equal to that of biological fluids (i.e., approximately the density of water), the mass of the tissue is treated implicitly because it is the same as the fluid now occupying that volume. Hence, the only force that the immersed boundary applies to the fluid arise from the elastic stress of the material. The filiform hairs of present interest, however, have a much higher density than the surrounding air, and an additional body force must be applied to the fluid to account for the inertia of the hairs and the force of gravity. One mechanism for handling the boundary mass is to locally increase the density of the fluid (i.e., air) so that it is equal to the mass of the immersed boundary, but this approach makes Fourier methods inapplicable [26]. Another approach, which is used here, is to introduce duplicate immersed boundary points (i.e., a second immersed boundary) with mass wherever it is needed. This *massive* boundary accounts for inertia and the gravitational force, and it is connected to the elastic boundary using a strong restoring force. In summary, there are two immersed boundaries, which are tightly linked together, with one boundary without mass representing the elastic forces in the solid and the other massive boundary representing the inertial and gravitation forces. A detailed derivation and analysis of this technique has been published elsewhere [11], and only the details relevant to modeling filiform hairs are presented below.

The body force per unit volume on the fluid, $\mathbf{f}$, is related to the force density in the immersed boundary, $\mathbf{F}$, by

$$\mathbf{f}(\mathbf{x},t) = \int \mathbf{F}(r,s,t)\delta(\mathbf{x}-\mathbf{X}(r,s,t))drds \ , \tag{5}$$

where δ is the 3-dimensional Dirac delta function, $\mathbf{x} = (x,y,z)$ are the fixed Cartesian coordinates (used for the fluid), and $\mathbf{X}(r,s,t)$ represents the 2-dimensional, transient immersed boundary in 3-dimensional space. Equation 5 is fundamental to the immersed boundary method because it handles the interaction between the moving immersed boundary and the fluid.

The immersed boundary force density can be divided into two parts: $\mathbf{F}_E$ representing the elastic stress force and $\mathbf{F}_K$ representing the inertial gravitational force. The elastic contribution is given by:

$$\mathbf{F}_E = -\frac{\partial E}{\partial \mathbf{X}} \ , \tag{6}$$

where $E(\mathbf{X})$ is the elastic energy function and $\mathbf{X}(r,s,t)$ is the location of the immersed boundary. We consider the immersed boundary as a 1-D rod (or a collection of 1-D rods woven to form a

2-dimensional surface) and use the following form for the energy functional:

$$E(\mathbf{X}) = \frac{1}{2}c_s \int \left(\left| \frac{\partial \mathbf{X}}{\partial s} \right| - 1 \right)^2 ds + \frac{1}{2}c_b \int \left(\frac{\partial^2 \mathbf{X}}{\partial s^2} \right)^2 ds \ , \tag{7}$$

where the first term, containing c_s, represents stretching or compression of the rod and the second term, containing c_b, represents the bending of the rod. Stretching of the filiform hairs is not significant in the problems of interest, so $c_s \gg c_b$ is used in the model. However, c_b is a parameter that must be determined from experimental data.

The second force on the immersed boundary, $\mathbf{F}_K$, represents the gravitational force, and it is incorporated using the massive immersed boundary. The equation for the massive immersed boundary is Newton's law ($\mathbf{F} = m\mathbf{a}$), and the only forces are gravity and a stiff spring force linking the massive and elastic immersed boundary. The location of the massive immersed boundary is given by $\mathbf{Y}(s, r, t)$, so Newton's law takes the form:

$$M(r, s)\frac{\partial^2 \mathbf{Y}}{\partial t^2} = -\mathbf{F}_K(r, s, t) - M(r, s)\mathbf{g} \ , \tag{8}$$

where $\mathbf{g}$ is the gravitational acceleration and $M(r, s)$ is the mass density of the immersed boundary. The massive and elastic boundaries are linked by stiff springs with zero rest length and spring constant K. Therefore, the force density for the massive boundary is

$$\mathbf{F}_K = K(\mathbf{Y}(r, s, t) - \mathbf{X}(r, s, t)) \ . \tag{9}$$

Larger values of K cause the two boundaries to be linked more closely, but K cannot be set to infinity. Suggested values for K and the accuracy implications of different values are discussed in [11].

In additional to matching the forces between the fluid and the immersed boundary, the velocity of the boundary must also be approximately equal to the velocity of the fluid. The velocity of the fluid, $\mathbf{u}(\mathbf{x})$, is based on an Eulerian reference frame, and it is defined on the fixed fluid grid. The immersed boundary is based on a Lagrangian reference frame, and its position is given by $\mathbf{X}(r, s, t)$. As with the forces described previously, a discrete form of the Dirac delta function is used handle

the interaction between the fluid and solid resulting in the following matching condition:

$$\frac{\partial \mathbf{X}(r,s,t)}{\partial t} = \int \mathbf{u}(\mathbf{x},t)\delta(\mathbf{x} - \mathbf{X}(r,s,t))d\mathbf{x} \ . \tag{10}$$

In summary, equations (2-10) are the full set of equations for the penalty immersed boundary method used here. The only significant, unknown parameter needed to model filiform hair motion is c_b, which must be determined from experimental data.

A number of different numerical approaches have been developed for approximately solving equations systems similar to the one presented in this section [21, 16, 17, 5]. The formal second-order method used here was originally described in [22] and [14], and a detailed application to the penalty immersed boundary method can be found in [11]. The term *formal* is used because full second-order accuracy is not achieved due to the jumps in the velocity derivative across the immersed boundary. We want to make two additionalremarks before briefly describing the algorithm: (1) forward differencing is used for the time derivatives and second-order accuracy is achieved using the midpoint rule so the algorithm presented below is completed twice per time step (i.e., second-order Runge-Kutta), and (2) second-order central finite differences are used for both first and second derivatives in space.

Numerical Algorithm. Given $\mathbf{u}$, $\mathbf{X}$, and $\mathbf{Y}$ from a previous solution or initial conditions, the following algorithm is repeated twice each time step.

1. Update the position of the massless boundary (equation 10).

2. Calculate the force density, which is the sum of the elastic force density (equation 6) and the massive boundary (equation 9).

3. Convert from the force density defined on the Lagrangian grid to forces applied to the Navier-Stokes equations on the Eulerian grid (equation 5).

4. Update the fluid velocity by solving the Navier-Stokes equations (2,3) using a Fast Fourier Transform (FFT). To accomplish this, the velocities from the previous time step are used in the nonlinear convection term $(\mathbf{u} \cdot \nabla \mathbf{u})$.

5. Update the massive boundary (equation 8).

The use of the FFT algorithm requires period boundary conditions. This is not a significant

limitation because we are able to immerse any boundary we require in the the fluid domain and impose 'inflow velocities' as described in the following section.

Application to Filiform Hairs

The model domain is a cuboid with a height of 3 mm, a depth of 3 mm, and a length of 6 mm. The finite difference nodes are equally spaced in all three dimensions, and a typical mesh has $32 \times 32 \times 64$ nodes if all the hairs are longer than 0.5 mm. If the hairs less than 0.5 mm are being modeled, a mesh with $64 \times 64 \times 128$ nodes is used. To check the accuracy of this mesh size, a few simulations were run with $128 \times 128 \times 256$ nodes, and they gave nearly identical results (i.e., hair deflections changed by less than 1%). Figure 3 shows the two different types of boundaries immersed in the fluid domain. The two-dimensional cylindrical surface represents the cerci, which is the antenna-like appendage at the rear of the abdomen. This boundary is treated as massless, and c_b and c_s for this boundary are set sufficiently high that the boundary does not move. In other words, this is a no-slip boundary immersed in the fluid domain. It is also important to note that this boundary does not extend out to the edges of the domain because then the no-slip condition would conflict with the uniform inflow velocity. The one-dimensional filiform hairs are attached slightly below the cerci surface and are sloped at approximately 80^o relative to the cerci surface. The hairs are massive with the mass density set to be that of water [10]. The two bottom nodes on the hair (nearest the center of the cerci) are fixed so that the hair cannot freely rotate without any associated energy cost. It is because of the two fixed nodes that the bottom of the hair is slightly below the surface of the cerci. Filiform hairs are placed in oval shaped asymmetrical sockets. The hair pivots in the sockets and the asymmetry of the sockets causes the hair to have a set plane of motion. This plane varies from hair to hair, but is conserved across animals. To limit the motion of the hairs to a single plane with a normal vector $\mathbf{n}$, the velocity of the fluid on the surface of the hair is projected onto the plane of allowed motion by

$$\mathbf{u}_p = \mathbf{u} - (\mathbf{u} \cdot \mathbf{n}). \tag{11}$$

This is the same approached used by Cummins et al. [3] for cricket filiform hairs. A similar solution for restricting the motion of the hair into a single plane is to significantly increase c_b to limit out of plane movement. Both approaches yielded similar results, but increasing c_b required smaller times

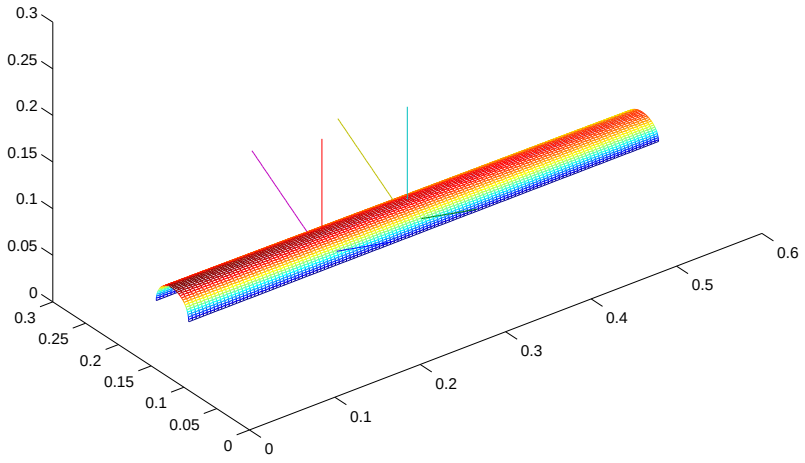

Figure 3: **Domain with Immersed Boundaries**. The fluid domain with an aspect ration of 1:1:2 and containing the two-dimensional cerci and one-dimensional filiform hairs of various lengths extending radially outward from the cerci.

for numerical stability so the projection method was normally used. Finally, the nodal spacing for the immersed boundaries are set to be less than half the nodal spacing in the fluid to avoid 'leaks'.

The inflow velocity is set by applying an external force per unit volume on the fluid that is equal to

$$\mathbf{f}_0(\mathbf{x},t) = \begin{cases} \alpha(\mathbf{u}_0(t) - \mathbf{u}(\mathbf{x},t)) & , \quad \mathbf{x} \in \Omega_0 \\ 0 & , \quad \text{otherwise} \ , \end{cases} \tag{12}$$

where $\mathbf{u}_0(t)$ is the desired velocity and Ω_0 is a set points on two grid planes on which we want to control the velocity. For the arthropods, we are typically interested in temporally oscillating velocities which may approximate velocities created by the flapping wings of a digger wasp as it approaches a cricket. As a result, $\mathbf{u}_0$ is typically defined by:

$$\mathbf{u}_0(t) = U \cdot \sin(2\pi\omega t) \tag{13}$$

where ω is the frequency of the oscillation and U is the peak velocity (e.g., 1 cm/s).

3 Results

The first set of numerical experiments were designed to determine the the bending strength of the cricket hair as a function of position along the length of the hair. This is the one unknown parameter in the model. It has been well established experimentally, that the hair is relatively rigid and bends primarily at the base and beneath the surface of the cerci. Based on a careful analysis of figure 4b, which shows a hair moving in an oscillating air environment, and the measurements of Kumagai et al. [12], we propose the following function to describe the bending strength of the cricket filiform hair:

$$c_b = \begin{cases} 0.002 & \text{if } x/L < 0.2 \\ 0.002 + 0.02(1 - \exp(-10(x/L - 0.2))) & \text{if } x/L \geq 0.2 \end{cases} \tag{14}$$

where x is the distance from the base of the hair in mm and L is the length of the hair, also in mm. This equation implies that most of the bending will occur near the base of the hair which is inside of the socket. In figure 4c, the model result is compared with an experimental measurement of hair motion. It is important to note that the hair in the model was exactly straight, but the hair in the experiment was bent, somewhat, causing some overlap error between the two results. However, we are still confident that the bending strength of the hair is reasonably accurate.

3.1 Single Hair Results

A number of experimental results have been published that examine the interaction between a single cricket filiform hair and an oscillating air field, and the immersed boundary model can be compared to these results. For these comparisons, we will establish a baseline model result and then compare the model predictions to experimental measurements while varying a single parameter in the model. The baseline model uses a 50 Hz oscillating air field with a peak velocity of 1.0 cm/sec, and the model domain has a single hair that is 0.7 mm in length. The first set of results, shown in figure 5, focus on the relationship between peak air velocity and the maximum angular deflection of the hair. The model predicts an approximately linear relationship, even when not using a log-log plot, which is not surprising considering the Reynolds number for the flow is very low. The grey

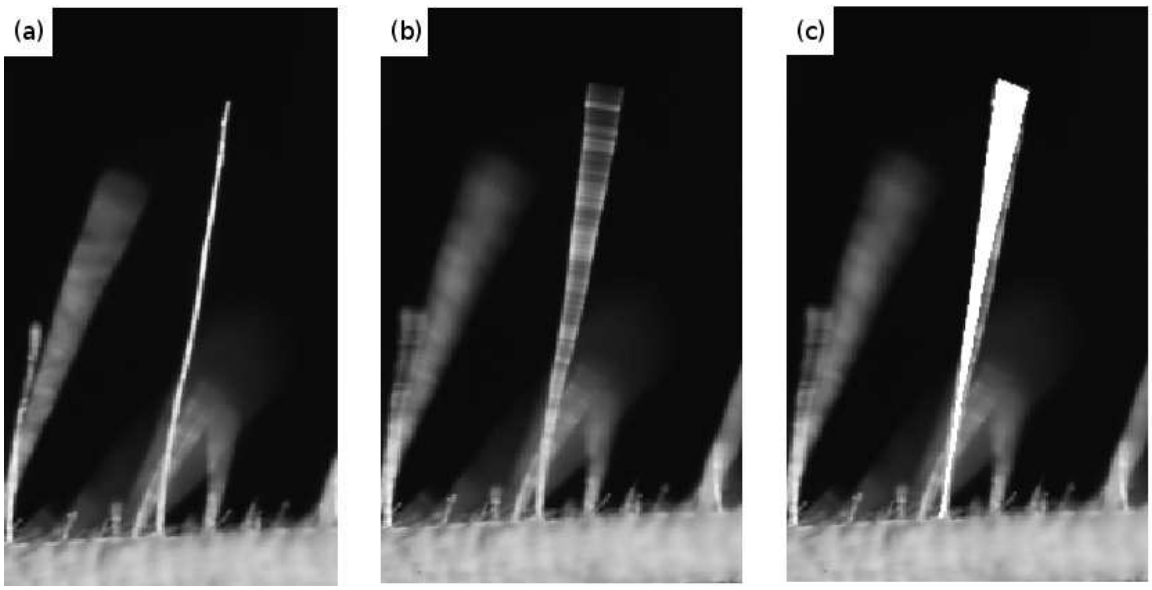

Figure 4: **Model versus Experimental Hair Motion**. (a) A single filiform hair at rest with the background hairs being out of focus. (b) A filiform hair in motion due to an oscillating air environment. (c) Model hair motion overlaying the experimental hair motion with part of the hair motion visible due to a bend in the experimental hair.

ovals in figure 5 show the approximate experimental results of Shimozawa and Kanou [23], which used a variety of hairs ranging in length from 0.2 mm to 1.3 mm. Overall, the agreement between the model and experiment are excellent. The model predicted almost no change in the phase shift between the oscillating hair and oscillating air field at different velocities. We are not aware of any published results examining this relationship, so it is unlikely that the phase shift depends significantly on the peak air velocity.

The second set of single hair results focuses on the effects changing the frequency of the air flow on the maximum deflection and phase shift of the hair. As shown in figure 6, the maximum deflection of the hair increases by a factor of approximately 3 when the frequency is increase from 20 Hz up to 100 Hz and the increase is greater at the lower frequencies. This result is in good agreement with Kumagai et al. [12], although there were minor differences between the experiment and model with regards to hair length and peak velocity. The model also predicts that the phase shift initially increases with increasing frequency before reaching an apparent plateau, as shown in figure 6. The experimental results of Kumagai et al. [12] also show an increase in phase shift, but at frequencies below 20 Hz (the 5-10 Hz range). Then, the experiments showed a decrease in the phase shift between 20 and 100 Hz. These qualitative difference lead to quantitative differences

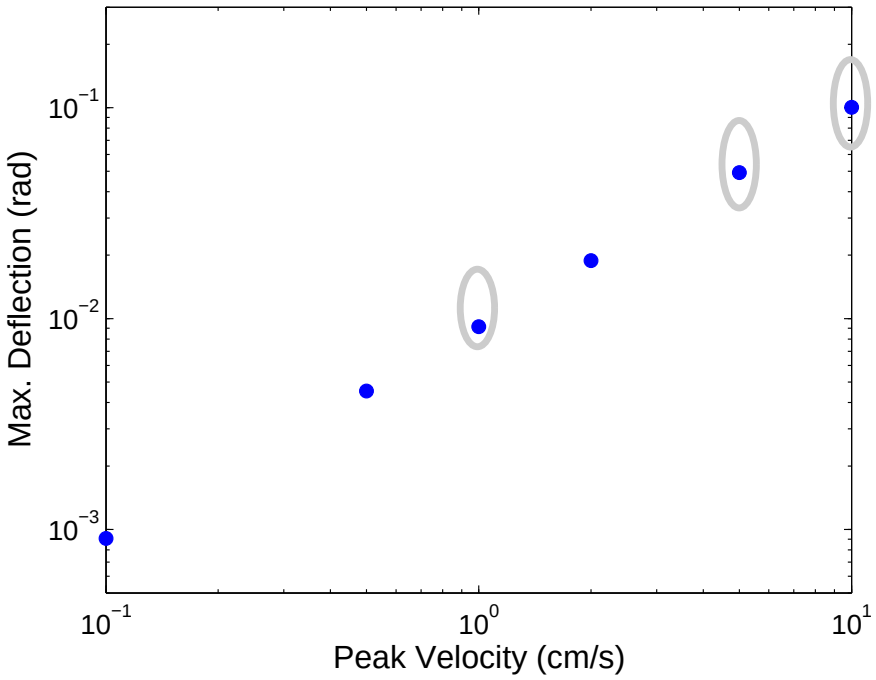

Figure 5: **Peak Velocity Dependence**. As the maximum velocity of the oscillating air increases, the maximum deflection increases linearly. The approximate experimental measurements from Shimozawa and Kanou [23] are shown in gray ovals.

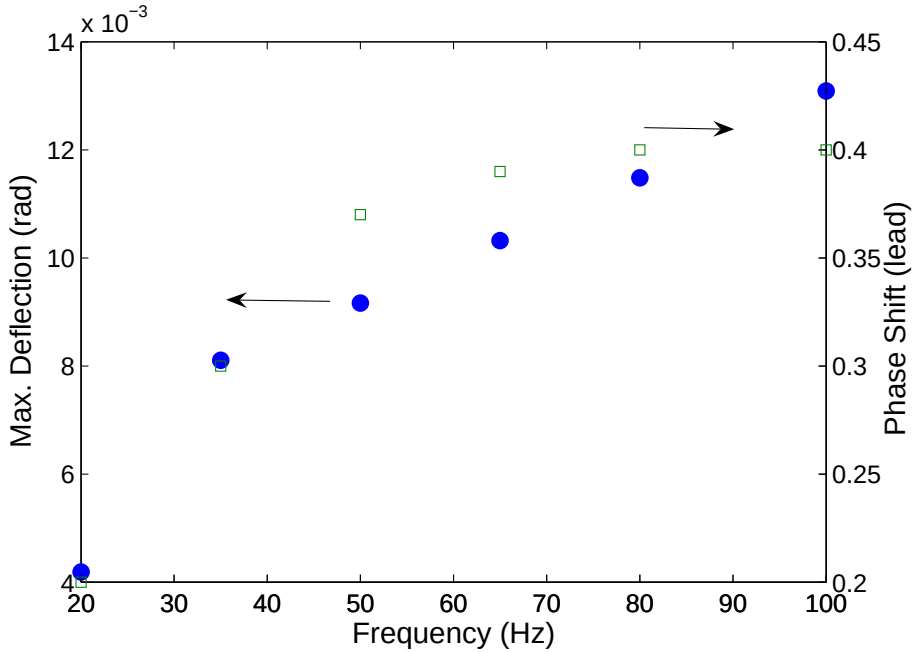

Figure 6: **Frequency Effects**. As the frequency of the oscillating air increases, the maximum deflection (solid circles) and phase shift (open squares, units are radians) also increase.

also. The model and experiment agree quantitatively at the low frequencies (20-50 Hz), but there are significant errors near 100 Hz where the model predicts of phase shift of 0.4 radians and the experiments had a phase shift near zero. There are a number of potential explanations for this discrepancy. First, the hair length and peak velocity used in the model were different from those used in the experiment. However, considering the near linearity of the flow, those difference are not enough to explain qualitative differences observed. Second, the assumption of incompressibility or the form of c_b used in the model could have impacted the modeling result. Ultimately, the models prediction of the phase shift is the correct order of magnitude (and often it is very close), and the variable is not one of primary concern, so the current error in phase shift at a relatively high frequencies in not a significant concern.

The final single hair result concerns the effects of hair length on the deflection and phase shift of the hair in an oscillating air field (50 Hz) with a peak velocity of 1 mm/sec. Figure 7(a) summarizes the effect of shortening or lengthening the baseline hair, which was 0.7 mm, on the maximum deflection of the hair. The solid dots represent the results of the immersed boundary simulation, and the grey ovals indicate the approximate experimental measurements from Shimozawa et al. [25]. The model predictions agree well with the experimental measurements except for the longest hair

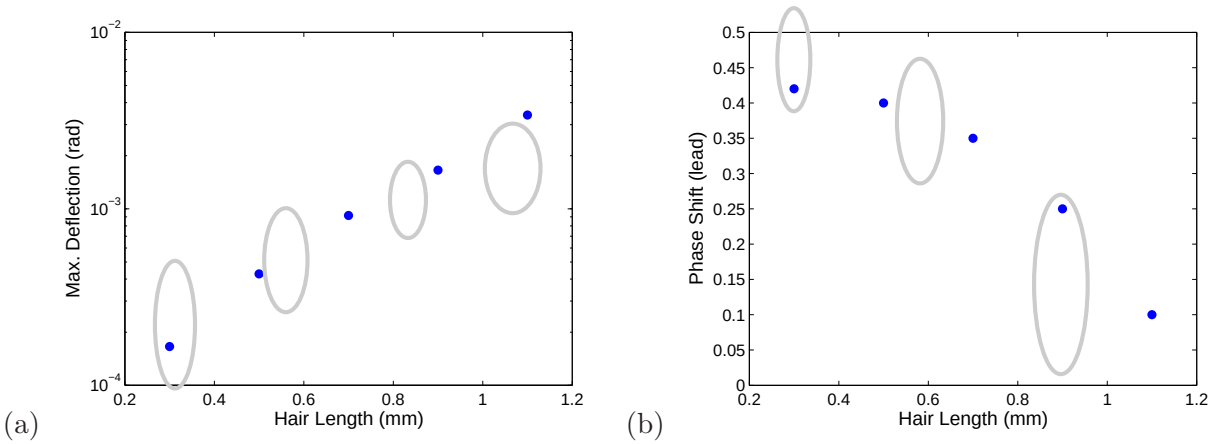

Figure 7: **Effects of Hair Length**. (a) The change in maximum hair deflection (solid circles) versus hair length, and (b) the change in phase shift (solid circles) versus hair length. In both (a) and (b), approximate experimental measurements from Shimozawa et al. [25] are shown in gray ovals.

modeled (1.1 mm). The most likely reason for this difference is that actual filiform hairs do not have uniform thickness, but they are thinner at the top and thicker at the bottom. This difference is amplified as the hairs get longer so that the model, which has hairs of uniform thickness, overestimates the drag on the upper parts of the hair and underestimates the rigidity of the the base. The difference between model and experiment results could be corrected by increasing c_b with length, but more experimental data is required to determine an accurate adjustment to the model. Figure 7(b) shows the effects of changing hair length on the phase shift of the hair relative to the oscillating air field. Again, the model prediction has good experiment with the experimental measurements except for a possible discrepancy at the longest hair length.

3.2 Multiple Hair Results

This section examines the impact of neighboring hairs on the motion of a specific hair in an oscillating air field. Following the work of Bathellier *et al.* [2] we define the coupling coefficient, κ, to be

$$\kappa = \frac{\theta_{ref} - \theta}{\theta_{ref}} \ , \tag{15}$$

where θ is the maximum deflection angle of the specific hair and θ_{ref} is the maximum deflection angle of that same hair without any other neighboring hairs on the cercus. In other words, κ is the fractional change in hair motion due to the presence of other hairs. Similarly, we define a fractional

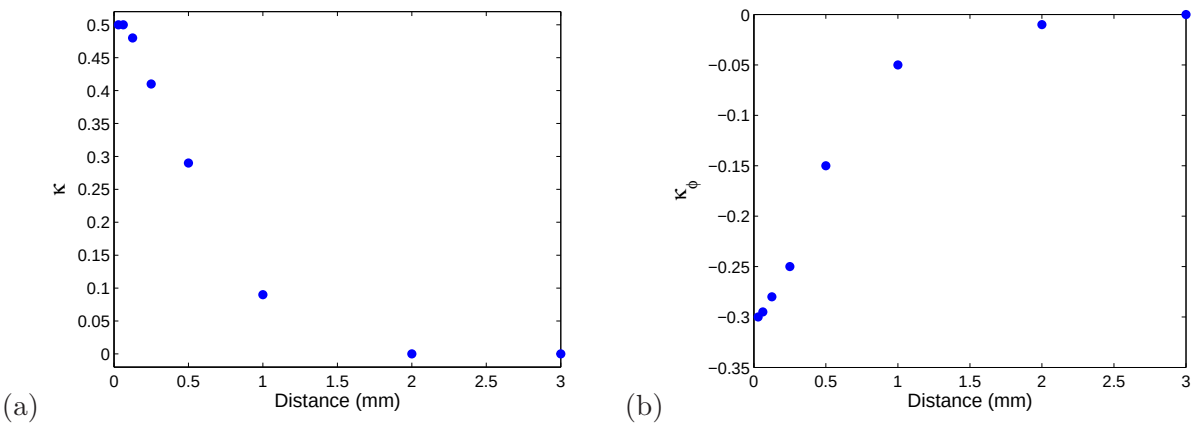

Figure 8: **Coupling between two free hairs**. As the distance between two hairs on cercus is decreased, there is (a) a fractional decrease, κ, in the maximum hair deflection, and (b) a fractional decrease, κ_ϕ, in the phase shift.

change in the phase shift, ϕ, as

$$\kappa_\phi = \frac{\phi_{ref} - \phi}{\phi_{ref}}. \tag{16}$$

For all multiple hair results presented here, the oscillating air field has a frequency of 50Hz and a peak velocity of 1 cm/sec.

For the first set of numerical experiments, two hairs were placed on the cercus, one directly down wind from the other, and both hairs could move freely in the direction of the air flow. Figure 8(a) shows the impact of changing the distance between the hairs on the fractional change in the maximum deflection angle, κ, and Figure 8(b) shows the fractional change in the phase shift for the same two hairs. These results show that as the two hairs move closer together, they begin to behave as a single 'super' hair with twice the stiffness of the individual hair and a greater phase shift. The maximum deflection angle of the hairs is halved when they are close together, and the phase shift increases by nearly 30%. The minimum hair-to-hair distance modeled is 0.03 mm, which is approximately 3-4 hair diameters. This is closer than long hairs are normally found on the cercus (cf, figure 1), but considering that longer hairs are sometimes within $0.2 - 0.5$ mm, this model predicts some viscous coupling occurs between the hairs.

The second set of multi-hair numerical experiments examined the effects of having a fixed hair on the cercus near a hair that was free to bend. In this case, the issue is once again the effects of the fixed, unbending hair on the free hair. Figure 9 shows that the fixed hair does decrease the motion of the flexible hair, but it is not as significant as as when both hairs are free to bend.

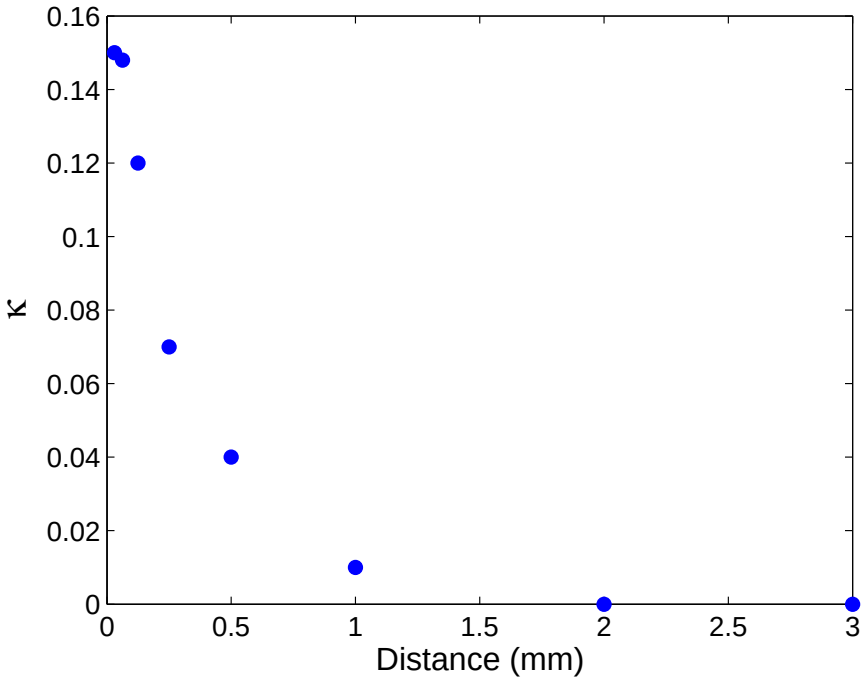

Figure 9: **Coupling between one free and one fixed hair**. As the distance between two hairs on cercus is decreased, there is a fractional decrease, κ, in the maximum hair deflection.

Essentially, the fixed hair, which is an infinitely thin 1-dimensional immersed boundary, acts to shelter the flexible hair slightly from the oscillating air field on one side, but it otherwise has little impact. Also, the phase shift of the flexible hair is reduced by less than 5% when the fixed hair is at the minimum distance modeled (0.03 mm). It should be noted that the hairs were not so close that they were able to contact each other. In summary, this immersed boundary model predicts that when a nearby hair is flexible, it has a greater impact on the neighboring hair than when it is fixed.

As mentioned in the introduction, Bathellier *et al.* [2] previously developed a model and performed experiments on the interaction of two filiform hairs on the leg of a spider. While the system they modeled is different from that considered here, some comparisons can be made between the two models. The previous two results are in some respects similar to the results of Bathellier *et al.*, and in other respects very different. First, both models predict that a neighboring hair can result in $\kappa = 0.5$ when the two hairs are within approximately 5 hair diameters (0.05 mm). Second, both models predict that the neighboring hair begins to have an impact when they are within 50-100 hair diameters ($0.5 - 1.0$ mm). However, Bathellier *et al.* predicted that having the second hair fixed

should have a much greater impact than when the second hair is free to move. This is obviously the opposite of what the model presented here predicts, so the question is, which is more accurate. First, the immersed boundary model predicts that when both hairs are flexible and very close, they behave as a single hair with half the deflection of an isolated hair. This makes sense physically, and the Bathellier model may under-predict the impact of a second flexible hair because the model uses an idealized flow field whereas the present model is dynamically (and approximately) solving the full Navier-Stokes equation which are mechanically coupled to (and influenced by) the hairs. On the other hand, the immersed boundary model presented here uses 1-dimensional hairs, which are infinitely thin, so it may under-predict the influence and sheltering effect of a neighboring, fixed hair. The 1-dimensional hair assumption can be avoided by modeling the hairs as immersed, 2-dimensional sheets wrapped in cylindrical shapes, but that would *significantly* increase the computational requirements of the model. Since a fixed hair is not a normal physical situation, modeling errors in this case are less of a concern. This model, as well as every other mathematical model, is only an approximation to the exact physics it is trying to describe, but we believe it is at least as accurate as other models that exist for modeling cricket filiform hairs.

The final set of numerical experiments examine the computation cost of modeling a large number of hairs. Our long-term goal is to model an entire cercus with approximately 1000 hairs. Figure 10 shows the computational cost for modeling a $6\ mm \times 3\ mm \times 3\ mm$ region of space for 1×10^5 time steps with different numbers of hairs on the surface of a section of a cercus. Each hair, regardless of length, consisted of 33 points in space. The simulations were all performed on a 3GHz Intel Xeon processor and none used more than 100 MB of memory. Figure 10 illustrates that the time to solve the Navier-Stokes equations without any hairs about 50 minutes total (or 0.03 sec per time step). Since the FFT method was used for solving the Navier-Stokes equations, the computational scalability follows the well established $n \log_2(n)$ behavior. In other words, doubling the domain size in each dimension, but maintain a fixed grid size, would increase the cost by a factor of about 24. The second piece of information contained in Figure 10 is that the computational cost varies linearly with the number of hairs and each hair requires approximately 2.7 minutes for the 1×10^5 time steps. To model the full cercus would require a 12-fold increase in the number of hairs and a 24-fold increase in the size of the fluid domain relative to the largest simulation shown here, which required 4.5 hours. This gives a predicted total of 54 days to simulate the entire cercus using the penalty immersed boundary method. Clearly, this is not impossible, but it is not practical at this

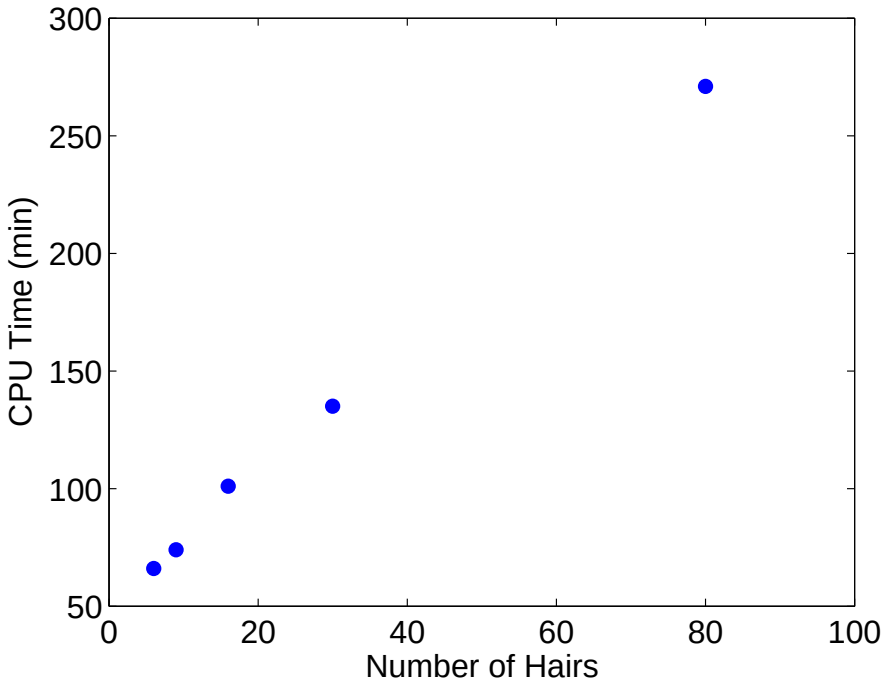

Figure 10: **Computational Scalability**. The computational time required for simulating 1×10^5 time steps with different numbers of hairs on the cercus.

time, especially for hypothesis testing. However, in the future we believe that a combination of faster computers and a parallel implementation should enable simulations of the full cercus in less than a day.

4 Conclusions

The penalty immersed boundary method is a new approach to modeling arthropod filiform hairs. The primary advantages of this method over other approaches are the ability to model large numbers of filiform hairs and the ability to use air flow from arbitrary direction. Further the full Navier-Stokes equations are solved, rather then their approximation. There are certain trade-offs which we need to do in order to achieve scalability of the calculation, most prominent one being the essential one-dimensionality of the hair. This may underestimate the effect of the standing hair on the flow and therefore on neighbooring hairs. Evethogh the nteraction between an imobile and mobile hair does not represent biologically relevant situation, one should be aware of this fact when using our model in different situations. Our modeling approach was shown to accurately capture

many of the previous experimental observations concerning the movement of a filiform hair in an oscillating air field. Further, we have examined the basic viscous coupling between two hairs at different distances. Our methodology hold the potential for modeling the full cercus with hundreds of filiform hairs, which can help answering fundamental questions about the design and function of the entire sensory system.

Acknowledgments

J.J.H. was supported by the Flight Attendants Medical Research Institute. B.C.K. was supported by the Fulton Undergraduate Research Initiative. T.G. was partially supported by NSF-CRCNS grant 0515290, NIH-NCRR grant PR16445 and NSF/NIH grant 0443863.

References

[1] F.G. Barth, U. Wastl, J.A.C. Humphrey, and R. Devarakonda. 1993. Dynamics of arthropod filiform hairs. ii. mechanical properties of spider trichobothria (cupiennius salei keys.). *Phil. Trans. R. Soc. Lond. B*, 340:445–461.

[2] B. Bathellier, F.G. Barth, J.T. Albert, and J.A.C. Humphrey. 2005. Viscosity-mediated motion coupling between pairs of trichobothria on the leg of the spider cupiennius salei. *J. Comp. Physiol. A*, 191:733–746.

[3] B. Cummins, T. Gedeon, I. Klapper, and R. Cortez. 2007. Interaction between arthropod filiform hairs ina fluid enviroment. *J. Theoretical Biol, to appear.*

[4] R. Devarakonda, F.G. Barth, and J.A.C. Humphrey. 1996. Dynamics of arthropod filiform hairs. iv. hair motion in air and water. *Phil. Trans. R. Soc. Lond. B*, 351:933–946.

[5] R. Dillon, L. Fauci, A. Fogelson, and D. Gaver. 1996. Modeling biofilm processes using the immersed boundary method. *J. Comput. Phys.*, 129:57–73.

[6] W. Gnatzy and R. HeuBlein. 1986. Digger wasp against crickets. i. receptors involved in the antipredator strategies of the prey. *Naturwissenschaften*, 73:212–215.

[7] W. Gnatzy and G. K amper. 1990. Digger wasp against crickets. ii. an airborne signal produced by a running predator. *J. Comp. Physiol. A*, 167:551–556.

[8] W. Gnatzy and R. Hustert R. *Mechanoreceptors in behavior.* Cornell University Press, Ithaca, NY, 1989.

[9] H.-G. Heinzel and M. Dambach. 1987. Travelling air vortex rings as potential communication signals in a cricket. *J. Comp. Physiol. A*, 160:79–88.

[10] J. Humphrey, R. Devarekonda, I. Iglesias, and F.G. Barth. 1993. Dynaics of arthropod filiform hairs. i. mathematical modelling of the hair and air motions. *Phil. Trans. R. Soc. Lond. B*, 340:423–444.

[11] Y. Kim. *The Penalty Immersed Boundary Method and its Applications to Aerodynamics.* PhD thesis, New York University, 2002.

[12] T. Kumagai, T. Shimozawa, and Y. Baba. 1998. Mobilities of the cercal wind-receptor hairs of cricket, *Gryllus bimaculatus*. *J. Comp. Physiol. A*, 183:7–21.

[13] T. Kumagai, T. Shimozawa, and Y. Baba. 1998. The shape of wind-receptor hairs of cricket and cockroach. *J. Comp. Physiol. A*, 183:187–192.

[14] M.-C. Lai and C.S. Peskin. 2000. An immersed boundary method with formal second-order accuracy and reduced numerical viscosity. *J. Comput. Phys.*, 160:705–719.

[15] M.A. Landolfa and J.P. Miller. 1995. Stimulus-response properties of cricket cercal filiform receptors. *J. Comp. Physiol. A*, 177:749–757.

[16] L. Lee and R.J. LeVeque. 2003. An immersed interface method for incompressible Navier–Stokes equations. *SIAM J. Sci. Comput.*, 25:832–856.

[17] W.K. Liu, Y.L. Liu, D. Farrell, L. Zhang, X.S. Wang, Y. Fukui, N. Patankar, Y.J. Zhang, C. Bajaj, J. Lee, J.H. Hong, X.Y. Chen, and H.Y. Hsu. 2006. Immersed finite element method and its applications to biological systems. *Comp. Meth. Appl. Mech. Eng.*, 195:1722–1749.

[18] R.M. Olberg and J.P. Miller JP. 1991. Behavioral measurements of directional resolution in the cricket cercal escape system. *Soc. Neurosci. Abst.*, 17:639.

[19] C.S. Peskin. 1977. Numerical analysis of blood flow in the heart. *J. Comput. Phys.*, 25:220–252.

[20] C.S. Peskin. 2002. The immersed boundary method. *Acta Numerica*, 11:479–517.

[21] C.S. Peskin and D.M. McQueen. 1995. A general method for the computer simulation of biological systems interating with fluids. *Symposia of the Society for Experimental Biology*, 49:265–276.

[22] C.S. Peskin and D.M. McQueen. *Heart Simulation by an Immersed Boundary Method with Formal Second-order Accuracy and Reduced Numerical Viscosity*. Kluwer Academic Publishers, 2001.

[23] T. Shimozawa and M. Kanou. 1984. The aerodynamics and sensory physiology of range fractionation in cercal filiform sensilla of the cricket gryllus bimaculatus. *J. Comp. Physiol. A*, 155:495–505.

[24] T. Shimozawa and M. Kanou. 1984. Varieties of filiform hairs: range fractionation by sensory afferents and cercal interneurons of a cricket. *J. Comp. Physiol. A*, 155:485–493.

[25] T. Shimozawa, T. Kumagai, and Y. Baba. 1998. Structural scaling and functional design of the cercal wind-receptor hairs of cricket. *J. Comp. Physiol. A*, 183:171–186.

[26] L. Zhu and C.S. Peskin. 2002. Simulation of a flapping flexible filament in a flowing soap film by the immersed boundary method. *J. Comput. Phys.*, 179:452–468.